

Cycle Slip Detection in the context of RTK GPS positioning of lightweight UAVs

C. Eling¹, E. Heinz¹, L. Klingbeil¹, H. Kuhlmann¹
¹Institute of Geodesy and Geoinformation, Universität Bonn

Abstract

In this paper a direct georeferencing system for the position and attitude determination of MAVs is presented. One important goal in the realization of this system is the development of tightly-coupled GPS algorithms, where the GPS raw measurements are directly fused with the observations of additional sensors, such as inertial sensors or cameras. The tightly-coupled algorithms are needed to improve the GPS processing in GNSS challenging environments. Since the development of these algorithms is not finished yet, this paper is focused on the cycle slip detection based on accelerometers in a Kalman filter. By means of a simple test it will be shown that the integration of accelerometers in the RTK GPS float solution allows for a reliable detection and repair of cycle slips.

Keywords

RTK GPS, UAV, direct georeferencing, cycle slip, Kalman filtering

1 INTRODUCTION

As a platform for mobile mapping applications, unmanned aerial vehicles (UAVs) are increasingly used in the recent years. Examples can be found in the fields of precision farming (Bendig et al. 2014), infrastructure inspection (Merz & Kendoul 2011) or surveying (Eisenbeiss et al. 2005). In comparison to land vehicles, UAVs have the advantage of being able to overfly inaccessible areas. Furthermore, they mostly allow for approaching an object from all viewing directions, without physical contact.

In the community, there is currently a discussion concerning the term for aerial vehicles. Beside the term “UAV” for example also the terms “drone”, “remotely piloted vehicle” and “remotely piloted aircraft” exist. This paper is dealing with the application of lightweight UAVs for mobile mapping. Since “lightweight UAV” is a very unspecific description, the term “micro aerial vehicle” (MAV) will be used instead of this throughout this paper. MAVs can generally be characterized having a weight limit of 5 kg and a size limit of 1.5 m (Eissenbeiss 2009).

Mobile mapping ordinarily requires a georeferencing of the collected mapping data. This georeferencing can be done directly or indirectly. Since spatial and time restrictions often exclude the possibility to deploy ground control points, a direct georeferencing, which is based on an onboard multi-sensor system, is often preferred. In this contribution a system for the direct georeferencing of MAVs is presented. This system has been realized within the research project *Mapping on Demand*. The goal of this research project is the development of an autonomously flying MAV, which is intended to be used for the 3D reconstruction of buildings. Among other sensors, the direct georeferencing system also includes an RTK (real-time kinematic) GPS system, to allow for cm-accuracy positioning of the mobile platform in real-time. However, the difficulty of using RTK GPS on an MAV is that the GPS measurement conditions are often challenging during flights, which leads to multipath effects, losses of lock (shadowing) and cycle slips in the carrier phase observations. This is especially true, when the MAV has to fly next to trees and close to building facades to collect well-suited images for a 3D reconstruction. To overcome this problem the development and implementation of a tightly-coupled RTK GPS algorithm is planned, where the observations of additional sensors, such as inertial sensors or cameras, are directly fused with the GPS raw measurements in a single filter. In doing so, the ambiguity re-initialization and the cycle slip detection can be improved significantly. To illustrate the positive impact of the integration of inertial sensors in the RTK GPS process, the issue of cycle slip detection using accelerometers will be addressed in this paper.

This paper is structured as follows: First, the developed direct georeferencing system and the MAV platform will be presented (section 2). In section 3 possibilities for the detection of cycle slips will be discussed. Afterwards, results of a simple test will be shown (section 4) and finally in section 5 an outlook on further developments will conclude this contribution.

2 THE SYSTEM DEVELOPMENT

Even if direct georeferencing is well known from airborne applications (e.g. Schwarz et al. 1993, Skaloud 1999, Heipke et al. 2002), the existing systems cannot easily be adopted for MAVs. The reasons for this are: (i) Due to challenging GNSS measurement conditions additional sensors (e.g. IMU (inertial measurement unit)) play a more important role for the position and attitude determination. (ii) The weight and the space of MAVs are strictly limited (e.g. 1.5 kg payload limitation), with the result that for example only lower quality IMUs can be used for MAV applications. On this account further lightweight sensors, such as stereo camera systems, are needed to bridge GPS losses of lock.

The possibility to include any additional sensor to the system is - apart from the space and weight limitations - a main reason for developing an own system instead of using a commercial unit with similar capabilities.

2.1 The direct georeferencing system

As mentioned before, the goal of this research was to develop a direct georeferencing system, which is customized for the use on MAVs. Generally, the system should have the following characteristics: (1) The weight of the system has to be less than 500g. (2) It should be real-time capable. (3) Outages of single sensors have to be bridgeable to allow for a reliable position and attitude determination independent on the measurement conditions. (4) The accuracies of the provided positions and attitudes should be better than 5 cm and 1 deg.

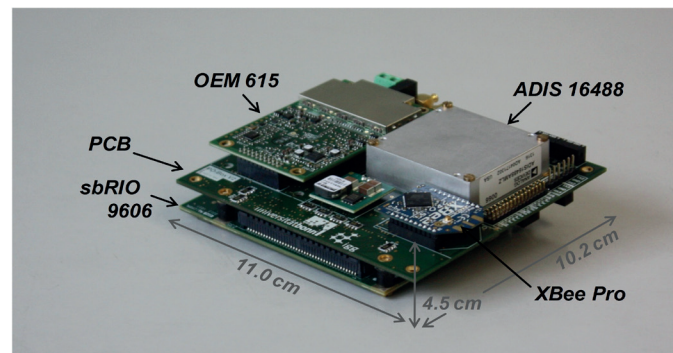


Figure 1: The direct georeferencing system with its components.

The developed direct georeferencing system is presented in Fig. 1. It consists of a Novatel OEM 615 GNSS receiver, a u-blox LEA6T L1-GPS receiver, an Analog Devices Adis 16488 IMU, a XbeePro 868 radio module and a National Instruments sbRIO 9606 real-time processing unit. Furthermore, an external interface allows for the integration of visual odometry data from stereo camera systems (Schneider et al. 2013). The dimensions of the system are 11.0 x 10.2 x 4.5 cm. The weight is roughly 240g, without the GPS antennas. More details to the system can be found in Eling et al. (2013).

All the algorithms running on the real-time processing unit are in-house developed. The reasons for this are: (a) The implemented software has to meet the requirements of the operating system that is running on the real-time processing unit. (b) The algorithms have to be well-suited to be applicable on an MAV platform in urban areas. (c) The final goal is the development of tightly-coupled GPS algorithms, where the raw observations of all sensors, including the stereo camera systems, should directly be fused in a single filter.

2.2 The MAV platform

Fig. 1 shows the current version of the developed MAV. In general it is based on the Mikrokoetter OktoXL construction kit from HiSystems. Beside the already mentioned georeferencing sensors the platform contains two stereo camera pairs (IDS uEye UI-1221LE) and a 5 Mpixel industrial camera (IDS uEye UI-2280SE). The stereo camera systems are on the one hand used for obstacle detection and on the other hand to provide visual odometry data. The industrial camera serves as the actual mapping sensor. Furthermore, a small computer performs the image processing and the flight planning onboard of the MAV.

The total weight of the system is 4.8 kg. Thus, it complies with the German law formalities (weight limit: 5 kg). Fig. 2 shows the current version of the MAV platform.

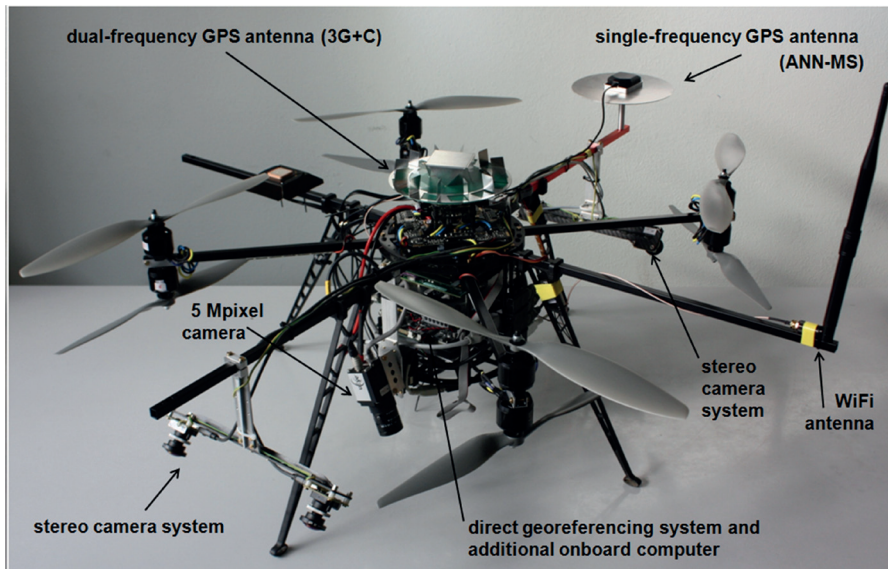


Figure 2: The modified UAV platform with the georeferencing and mapping sensors.

3 RTK GPS AND CYCLE SLIPS

As already mentioned in the introduction, the positioning of the MAV is mainly based on RTK (real-time kinematic) GPS. RTK GPS is a relative positioning procedure, based on GNSS carrier-phase observations, which allows for the determination of the vector between a mobile rover and a stationary master station in real-time.

The mathematical model for carrier phase measurements is given by (Hofmann-Wellenhof et al. 2008):

$$\Phi^j(t) = \frac{1}{\lambda} \rho^j(t) + N^j + \frac{c}{\lambda} \Delta\delta^j(t) + \frac{1}{\lambda} \zeta^j + \varepsilon^j, \quad (1)$$

where $\Phi^j(t)$ is the carrier phase from the satellite j at the time t , expressed in cycles. λ is the wavelength. $\rho^j(t)$ is the geometric range and N^j is the ambiguity that is inherently integer. $\Delta\delta^j$ is the combined satellite and receiver clock bias and c is the speed of light. Finally, the term ζ^j includes all the remaining range biases, such as the atmospheric refractions. The term ε^j denotes the measurement noise.

Due to a single-differencing (SD) and double-differencing (DD) of the observations, several biases, such as atmosphere refractions, satellite orbit errors as well as satellite or receiver clock biases can be reduced significantly or even eliminated. In doing so, centimetre positioning accuracies can be achieved.

When considering equation (1) more carefully, one important characteristic of GNSS receivers can be seen: the ambiguity parameter is time-independent. The reason for this is that once the GNSS receiver is turned on, the receiver initializes an integer counter. Afterwards, during the tracking, this counter is incremented, whenever the fractional carrier phase changes from 2π to 0. Thus, combining the integer counter and the fractional part, the receiver can always provide the observed accumulated carrier phase. The initial and unknown integer number of cycles N between the satellite and the receiver keeps constant. This relation is also presented in Fig. 3 (left). Thus, the carrier phase ambiguity remains constant as long as no loss of the signal lock occurs (Hofmann-Wellenhof et al. 2008).

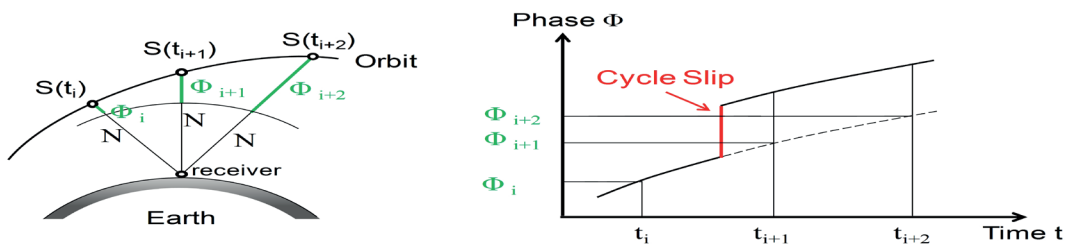


Figure 3: Representation of a carrier phase measurement (left) and of a cycle slip (right) (mod. Hofmann-Wellenhof et al. 2008)

In case the receiver loses the signal lock, the integer counter is re-initialized, as soon as the corresponding satellite signal is visible again. Since the re-initialized integer counter is usually different from the initial integer counter a jump in the accumulated phase arises. This jump is called a cycle slip (see Fig. 3, right).

The reasons for the occurrence of cycle slips are diverse. Mostly, cycle slips arise due to a signal interruption or a temporary obstruction of single satellite signals. Other reasons can be a poor signal to noise ratio caused by ionospheric refractions, multipath, low satellite elevations or high receiver dynamics.

3.1 Cycle slip detection using phase combinations or the LTI

The reliable detection of cycle slips is very important, since undetected cycle slips would lead to biases in the carrier phase measurements, with the result that cm-accuracies would no longer be achievable.

One possibility to detect cycle slips is to approximate the carrier phase progression with a low-order polynomial. However, for a real-time processing this is not useful. The reason is that many carrier phase measurements are needed for the approximation of the phase progression.

Another well known possibility to detect cycle slips is the use of phase combinations. The idea is that biases or the receiver-satellite-geometry can be eliminated from the phase observations due to a differencing. In this way, cycle slips become more visible. Particularly the geometry-free phase combination, which is the difference between the carriers on two frequencies (see equation (2)), is suitable for the cycle slip detection (Hofmann-Wellenhof et al. 2008).

$$\Phi_1(t) - \frac{f_1}{f_2} \Phi_2(t) = N_1 - \frac{f_1}{f_2} N_2 - \frac{b(t)}{f_1} \left(1 - \frac{f_1^2}{f_2^2} \right) \quad (2)$$

The only time-varying quantity on the right side of equation (2) is the ionospheric residual $b(t)$. Assuming that changes in the ionosphere refraction are small between two epochs the geometry-free phase combination should be constant. On this account, cycle slips can be detected easily, if the geometry-free phase combination exceeds a given threshold.

With this procedure it is also possible to determine whether the cycle slip comes from the L1 or the L2 frequency. However, disadvantages of the procedure are that (i) dual-frequency GNSS data is required, with the result that the procedure cannot be used for low-cost single-frequency GPS data and (ii) the procedure is not able to detect all combinations of cycle slips (Bisnath 2000).

Most of the GNSS receivers also provide a lock time indicator (LTI) to the user. Once the oscillator of the receiver is locked to the satellite signal it continues to follow the phase of the carrier with a high frequency (Langley 1991). Then, the LTI is the elapsed time since the satellite signal is locked. Thus, once the LTI is smaller than in the previous epoch, the integer counter has been re-initialized and a cycle slip is detected.

Together, the geometry-free phase combination and the LTI provide reliable detection methods for cycle slips. However, it cannot be excluded that cycle slips remain undetected only applying these procedures. Furthermore, cycle slips not only have to be detected, but also have to be repaired. For the repair of cycle slips the geometry-free phase combination and the LTI are not well-suited.

3.2 Cycle slip detection and repair using inertial measurements

In the case that knowledge about the motion behaviour of the rover or observations from additional sensors are available, cycle slips can also be detected using a Kalman filter (e.g. Bastos & Landau 1988). Since the presented MAV is very dynamic and it can move in every direction rapidly, it is not easy to find an appropriate dynamical model for this MAV. However, the used direct georeferencing system comprises of inertial sensors, such as accelerometers. Certainly, these sensors have to be integrated two times to predict the rover position. However, within two GPS measurement epochs (e.g. 0.1 s) drift effects are negligible. On this account, the accelerometers are well suited to detect cycle slips in the GPS carrier phase measurements.

Usually, GPS positions are represented in the e-frame (earth-centred, earth-fixed, ECEF). Since accelerometers measure in the IMU sensor frame, the observed accelerometers have to be rotated into the e-frame. Furthermore, the gravitational acceleration has to be taken into account, when using accelerometers for the prediction of GPS positions. This is generally done by applying a strapdown algorithm (see e.g. Jekeli 2001). To simplify the problem in this paper, it is assumed here that (a) the IMU sensor system is aligned with the b-frame (body frame) of the mobile platform, (b) the rotation from the b-frame to the e-frame is known and (c) the gravitational accelerations can be eliminated from the measurements:

$$\ddot{\mathbf{r}}_p^e(t) = \mathbf{g}^e(r_p(t)) + \mathbf{a}_p^e(t), \quad (3)$$

where \mathbf{g} is the gravitational acceleration and $\mathbf{a}_p^e(t)$ includes the measured specific forces, represented in the e-frame at the time t and point P . \mathbf{r} is the position. The resulting accelerations are used as a control input in a Kalman filter. Thus, the system dynamics model of the GPS float solution is:

$$\bar{\mathbf{x}}_{k+1} = \mathbf{T}_k^{k+1} \cdot \hat{\mathbf{x}}_k + \mathbf{B}_k^{k+1} \cdot \mathbf{u}_k = \begin{bmatrix} \mathbf{I}_{3 \times 3} & \mathbf{I}_{3 \times 3} \cdot \Delta t & \mathbf{0} & \mathbf{0} \\ \mathbf{0} & \mathbf{I}_{3 \times 3} & \mathbf{0} & \mathbf{0} \\ \mathbf{0} & \mathbf{0} & \mathbf{I}_{n \times n} & \mathbf{0} \\ & & & \mathbf{I}_{n \times n} \end{bmatrix} \cdot \hat{\mathbf{x}}_k + \begin{bmatrix} \mathbf{I}_{3 \times 3} \cdot \Delta t^2 \\ \mathbf{I}_{3 \times 3} \cdot \Delta t \\ \mathbf{0} \\ \mathbf{0} \end{bmatrix} \cdot \mathbf{u}_k. \quad (4)$$

The state vector consists of the rover position \mathbf{r} , the rover velocity $\dot{\mathbf{r}}$ and the SD ambiguity parameters N on the GPS L1 and the GPS L2 frequency:

$$\mathbf{x} = [r_{R,x} \ r_{R,y} \ r_{R,z} \ \dot{r}_{R,x} \ \dot{r}_{R,y} \ \dot{r}_{R,z} \ N_{R,L1}^1 \dots N_{R,L1}^n \ N_{R,L2}^1 \dots N_{R,L2}^n]^T. \quad (5)$$

The observation vector \mathbf{l} includes DD carrier phases Φ and DD pseudoranges P :

$$\mathbf{l} = [\Phi_{R,L1}^{1k} \dots \Phi_{R,L1}^{nk} \ \Phi_{R,L2}^{1k} \dots \Phi_{R,L2}^{nk} \ P_{R,L1}^{1k} \dots P_{R,L1}^{nk} \ P_{R,L2}^{1k} \dots P_{R,L2}^{nk}]^T \quad (6)$$

and the vector \mathbf{u} consists of the accelerations $\ddot{\mathbf{r}}$. Cycle slips can now be detected considering the innovation:

$$\mathbf{d}_{k+1} = \mathbf{l}_{k+1} - \mathbf{H}_{k+1} \cdot \bar{\mathbf{x}}_{k+1}, \quad (7)$$

where the design matrix \mathbf{H} represents the nonlinear functional model for a single baseline (one master, one rover) (see e.g. Eling et al. 2014 or Takasu & Yasuda 2009).

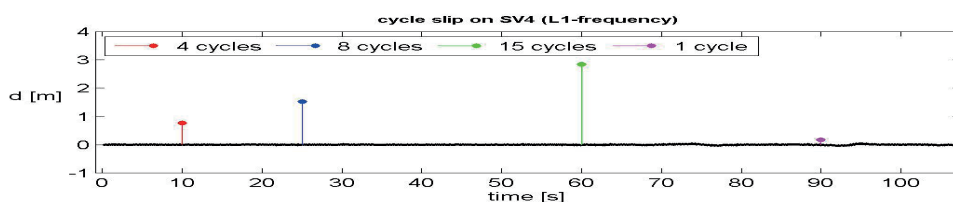
In case there exist no cycle slips in the carrier phases, the innovation remains close to zero. Thus, when the innovation exceeds a threshold $d > \beta$ (e.g. $\beta \approx 0.1-0.15$ m), a cycle slip is probably the reason.

In general, there are different possibilities to deal with detected cycle slips, but in the first instance there is a need to clarify whether the cycle slip comes from the reference satellite, which is the satellite used for the DD determination, or another satellite. Since a cycle slip on the carrier phase of the reference satellite would lead to large innovations for all DD observations these both cases can easily be distinguished.

After a cycle slip has been detected, the SD ambiguity parameter in the state vector can be re-initialized. As it will be shown in the results (section 4), it is also possible to directly repair the carrier phases or the fixed ambiguities based on the innovations.

4 TEST

In a simple test scenario the Kalman filter cycle slip detection was tested. During a drive in urban areas, GPS data and IMU data were recorded with rates of 10 and 1000 Hz using Leica 1200 GPS devices and an high-grade IMU from Imar (iNAV-FJI-LSURV-001), which provides very precise accelerations. Afterwards, the recorded data was analyzed in a postprocessing step. As already mentioned in section 3.2, the accelerations were first rotated into the e-frame and corrected by the gravitational acceleration. Finally, the GPS raw measurements and the accelerations were filtered in the presented Kalman filter. Since there were no real cycle slips available in this test, cycle slips were simulated on both GPS frequencies.



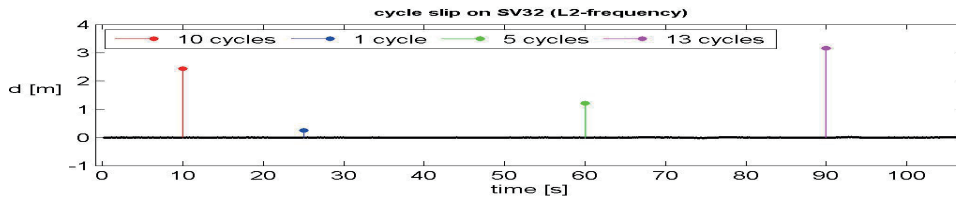


Figure 4: The innovations for the DD carrier phase observations of the reference satellite and the satellites 4 and 32 during the test drive. The simulated cycle slips can be seen clearly (coloured dots).

In Fig. 4 the innovations for the L1 DD carrier phase observations of the reference satellite and the satellite 4 as well as the L2 DD carrier phase observations of the reference satellite and satellite 32 are presented. The extent of the innovations depends on the measurement conditions, but ordinarily, the innovations do not exceed 5 cm (black dots). In contrast in the epochs where cycle slips were added to the measurements, significant outliers can be seen in the innovations of the respective satellites (coloured dots).

Table 1: Results of the detection of simulated cycle slips

SV	frequency	# cycles	Innovation [m]	Innovation [cycles]
4	L1 ($\lambda \approx 19.05\text{cm}$)	4	0.760	$3.9906 \approx 4$
		8	1.523	$7.9958 \approx 8$
		15	2.840	$14.9081 \approx 15$
		1	0.174	$0.9118 \approx 1$
32	L2 ($\lambda \approx 24.45\text{ cm}$)	10	2.442	$9.9857 \approx 10$
		1	0.243	$0.9955 \approx 1$
		5	1.220	$4.9885 \approx 5$
		13	3.168	$12.9554 \approx 13$

In Table 1 the results of different simulated cycle slips are shown. Thus, the cycle slips are not only conspicuous, but their extent is quite similar to the input. Therefore, cycle slips can be detected very reliably and the results from the innovation test are obviously also well-suited to repair cycle slips.

5 CONCLUSION AND OUTLOOK

In this paper a direct georeferencing system for the position and attitude determination of MAVs has been presented. One important goal in the realization of this system is the development of tightly-coupled GPS algorithms, which are needed to improve the GPS processing in GNSS challenging environments. As an example for the positive impact of inertial sensors on the RTK GPS algorithms, the cycle slip detection based on accelerometers was chosen in this contribution. Results of a simple test have shown that the integration of accelerometers in the RTK GPS float solution allows for a reliable detection of cycle slips.

Currently, the authors are working on the development of a full-motion state tightly-coupled strapdown algorithm, where GPS observations are fused with angular rates, accelerations, magnetic field observations and visual odometry data from stereo camera systems. Using this sensor fusion the ambiguity resolution and the cycle slip detection will be improved significantly for MAV flights.

ACKNOWLEDGEMENTS

This work was funded by the DFG (Deutsche Forschungsgemeinschaft) under the project number 1505 “Mapping on Demand”. The authors wish to express their gratitude for that.

REFERENCES

- BASTOS, L. & LANDAU, H. (1988): Fixing cycle slips in dual-frequency kinematic GPS-applications using Kalman filtering, *Manuskripta Geodaetica*, 13, 4, pp. 249-256
- BENDIG, J. BOLTON, A., BARETH, G. (2013): UAV-based Imaging for Multi-Temporal, very high Resolution Crop Surface Models to monitor Crop Growth Variability, *PFG*, 6/2013, pp. 551-562
- BISNATH, S. B. (2000): Efficient, automated cycle-slip correction of dual-frequency kinematic GPS data. In: *ION GPS 2000*, Salt Lake City, Utah, pp 145-154
- EISENBEISS, H. & LAMBERS, K. & SAUERBIER, M., (2005): Photogrammetric recording of the archaeological site of pinchango alto (palpa, peru) using a mini helicopter (UAV). *The World is in Your Eyes - Proceedings of the 33rd CAA Conference*.
- EISSENBEISS, H. (2009): UAV Photogrammetry. Dissertation, ETH Zurich No. 18515
- ELING, C., KLINGBEIL, L., WIELAND, M. & KUHLMANN, H. (2013): A precise position and attitude determination system for lightweight aerial vehicles. *Int. Arch. Photogramm, Remote Sens. Spatial Inf. Sci.*, XL-1/W2, 201-206
- ELING, C. & KLINGBEIL, L. & KUHLMANN, H., (2014): Development of an RTK-GPS system for precise real-time positioning of lightweight UAVs, In proc. of: *Ingenieurvermessungskurs 2014*, Zürich, pp 111-123.
- HEIPKE, C. & JACOBSEN, K. & WEGMANN, H. (2002): Integrated Sensor Orientation -Test report and workshop proceedings, OEEPE Official Publication, Vol.43, Frankfurt a.M.
- HOFMANN-WELLENHOF, B., LICHTENEGGER, H. & WASLE, E. (2008): *GNSS Global Navigation Satellite Systems*. Springer-Verlag Wien New York, ISBN 978-3-211-73012-6
- JEKELI, C. (2001): *Inertial Navigation Systems with Geodetic Applications*, Walter de Gruyter, Berlin - New York
- LANGLEY, R.B. (1991): The GPS Receiver: An introduction, *GPS World*, January 1991, pp. 50-53
- MERZ, T. & KENDOUL, F., (2011): Beyond visual range obstacle avoidance and infrastructure inspection by an autonomous helicopter. *Proceedings of the IEEE/RSJ International Conference on Intelligent Robots and Systems, IROS 2011*, San Francisco, USA.
- SCHNEIDER, J. & LÄBE, T. & FÖRSTNER, W., (2013): INCREMENTAL REAL-TIME BUNDLE ADJUSTMENT FOR MULTI-CAMERA SYSTEMS WITH POINTS AT INFINITY, *INT. ARCH. PHOTOGRAMM. REMOTE SENS. SPATIAL INF. SCI.*, XL-1/W2, 355-360.
- SCHWARZ, K.P. & CHAPMAN, M. & CANNON, M. & GONG, P. (1993): An integrated INS/GPS approach to the georeferencing of remotely sensed data, *Photogramm Eng Rem S* 49, 11, pp. 1667-1674
- ŠKALOUD, J. (1999): *Optimizing Georeferencing of Airborne Survey Systems by INS/DGPS*. PhD thesis, University of Calgary
- TAKASU, T. & YASUDA, A. (2009): Development of the low-cost RTK-GPS receiver with an open source program package RTKLIB. *Intern. Symp. on GPS/GNSS 2009, ICC Jeju*, Korea

Contact:

M.Sc. Christian Eling,

Institute of Geodesy and Geoinformation, Universität Bonn

Nussallee 17, D-53115 Bonn, Germany

Email: eling@igg.uni-bonn-de